ACADEMIC OPEN INTERNET JOURNAL WWW.ACADJOURNAL.COM VOLUME 16 2005

ANALYSIS OF SEGMENTATION OF CHROMOSOME SPREAD IMAGES USING STANDARDIZED PARAMETERS IN DISCRETE CONSINE TRANSFORM BASED GRADIENT VECTOR FLOW ACTIVE CONTOURS

A.Prabhu Britto[1] and Dr.G.Ravindran[2]

[1]*Center for Medical Electronics, Department of Electronics and Communication Engineering, Anna University, Chennai 600025 INDIA britto_albert@ieee.org*
[2]*Chairman, Faculty of Information and Communication Engineering, Anna University, Chennai 600025 INDIA*

ABSTRACT
In this research, characterization of Discrete Cosine Transform (DCT) based Gradient Vector Flow (GVF) Active Contours as a boundary mapping technique for chromosome spread images is done. Statistical testing validates the experimental results of characterization. Investigations on a different dataset are carried out to validate the characterized parameters that govern the formulation of the DCT based GVF Active Contour and the parameters are standardized. Further experiments are carried out to evaluate the validity of the standardization using another dataset. Results indicate that the DCT based GVF Active Contours are an efficient tool for boundary mapping of chromosome spread images.

Keywords: Gradient Vector Flow, Active Contours, Chromosome, Boundary Mapping, Characterization, Standardization

1. INTRODUCTION

This research work used Discrete Cosine Transform (DCT) based Gradient Vector Flow (GVF) Active Contours to obtain accurate segmentation (boundary mapping) results from a class of chromosome spread images having variability in shape, size and other image properties.

The classical boundary mapping techniques, namely, region growing, relaxation labeling, edge detection and linking suffer from limitations. Usage of only local information may lead to incorrect assumptions during the boundary integration process leading to errors. Noise and artifacts can possibly cause incorrect segmentation or boundary discontinuities in segmented objects[14].

Active Contours or Deformable Curves is a high-level boundary mapping technique with the main advantage of being able to generate closed parametric curves from images. The incorporation of a smoothness constraint provides robustness to noise and spurious edges. The focus is on parametric deformable curves, which provide a compact, analytical description of object shape. A class of parametric Active Contours called Gradient Vector Flow (GVF) field Active Contours is chosen for boundary mapping in chromosome spread images.

2. ACTIVE CONTOUR MODELS

Active Contours also called as Snakes or Deformable Curves, first proposed by Kass[13] are energy minimizing contours that apply information about the boundaries as part of an optimization procedure. They are generally

initialized by automatic or manual process around the object of interest. The contour then deforms itself iteratively from its initial position in conformity with nearest dominant edge feature, by minimizing the energy composed of the Internal and External forces, converging to the boundary of the object of interest. The Internal forces computed from within the Active Contour enforce smoothness of the curve and External forces derived from the image, help to drive the curve toward the desired features of interest during the course of the iterative process.

The energy minimization process can be viewed as a dynamic problem where the active contour model is governed by the laws of elasticity and lagrangian dynamics[8], and the model evolves until equilibrium of all forces is reached, which is equivalent to a minimum of the energy function. The energy function is thus minimized, making the model active.

3. FORMULATION OF ACTIVE CONTOUR MODELS

An Active Contour Model can be represented by a curve **c**, as a function of its arc length t,

$$c(t) = \begin{pmatrix} x(t) \\ y(t) \end{pmatrix} \quad \text{-- (1)}$$

with t = [0…1]. To define a closed curve, c(0) is set to equal c(1). A discrete model can be expressed as an ordered set of n vertices as $v_i = (x_i, y_i)^T$ with $v=(v_1,\ldots,v_n)$. The large number of vertices required to achieve any predetermined accuracy could lead to high computational complexity and numerical instability[8].

Mathematically, an active contour model can be defined in discrete form as a curve $x(s) = [x(s), y(s)], se[0,1]$ that moves through the spatial domain of an image to minimize the energy functional

$$E = \int_0^1 \frac{1}{2}(a \mid x'(s) \mid^2 + b \mid x''(s) \mid^2) + E_{ext}(x(s))ds \quad \text{-- (2)}$$

where a and ß are weighting parameters that control the active contour's tension and rigidity respectively[5]. The first order derivative discourages stretching while the second order derivative discourages bending. The weighting parameters of tension and rigidity govern the effect of the derivatives on the snake.

The external energy function E_{ext} is derived from the image so that it takes on smaller values at the features of interest such as boundaries and guides the active contour towards the boundaries. The external energy is defined by

$$E_{ext} = k \mid G_s(x,y) * I(x,y) \mid \quad \text{-- (3)}$$

where, $G_s(x,y)$ is a two-dimensional Gaussian function with standard deviation s, I(x,y) represents the image, and ? is the external force weight. This external energy is specified for a line drawing (black on white) and positive ? is used. A motivation for applying some Gaussian filtering to the underlying image is to reduce noise. An active contour that minimizes E must satisfy the Euler Equation

$$ax''(s) - bx''''(s) - \nabla E_{ext} = 0 \quad \text{-- (4)}$$

where $F_{\text{int}} = ax''(s) - bx''''(s)$ and $F_{ext} = -\nabla E_{ext}$ comprise the components of a force balance equation such that

$$F_{\text{int}} + F_{ext} = 0 \quad \text{-- (5)}$$

The internal force F_{int} discourages stretching and bending while the external potential force F_{ext} drives the active contour towards the desired image boundary. Eq.(4) is solved by making the active contour dynamic by treating x as a function of time t as well as s. Then the partial derivative of x with respect to t is then set equal to the left hand side of Eq.(4) as follows $x_t(s,t) = ax''(s,t) - bx''''(s,t) - \nabla E_{ext}$ -- (6)

A solution to Eq.(6) can be obtained by discretizing the equation and solving the discrete system iteratively[13]. When the solution x(s,t) stabilizes, the term $x_t(s,t)$ vanishes and a solution of Eq.(4) is achieved.

Traditional active contour models suffer from a few drawbacks. Boundary concavities leave the contour split across the boundary. Capture range is also limited. Methods suggested to overcome these difficulties, namely multiresolution methods[2], pressure forces[11], distance potentials[12], control points[3], domain adaptivity[4], directional attractions[1] and solenoidal fields[10], however solved one problem but introduced new ones[6]. Hence, a new class of external fields called Gradient Vector Flow fields [6, 7] was suggested to overcome the difficulties in traditional active contour models.

4. GRADIENT VECTOR FLOW (GVF) ACTIVE CONTOURS

Gradient Vector Flow (GVF) Active Contours use Gradient Vector Flow fields obtained by solving a vector diffusion equation that diffuses the gradient vectors of a gray-level edge map computed from the image. The GVF active contour model cannot be written as the negative gradient of a potential function. Hence it is directly specified from a dynamic force equation, instead of the standard energy minimization network. The external forces arising out of GVF fields are non-conservative forces as they cannot be written as gradients of scalar potential functions. The usage of non-conservative forces as external forces show improved performance of Gradient Vector Flow field Active Contours compared to traditional energy minimizing active contours[6, 7].

The GVF field points towards the object boundary when very near to the boundary, but varies smoothly over homogeneous image regions extending to the image border. Hence the GVF field can capture an active contour from long range from either side of the object boundary and can force it into the object boundary. The GVF active contour model thus has a large capture range and is insensitive to the initialization of the contour. Hence the contour initialization is flexible.

The gradient vectors are normal to the boundary surface but by combining Laplacian and Gradient the result is not the normal vectors to the boundary surface. As a result of this, the GVF field yields vectors that point into boundary concavities so that the active contour is driven through the concavities. Information regarding whether the initial contour should expand or contract need not be given to the GVF active contour model. The GVF is very useful when there are boundary gaps, because it preserves the perceptual edge property of active contours[13, 7].

The GVF field is defined as the equilibrium solution to the following vector diffusion equation[6],

$$u_t = g(|\nabla f|)\nabla^2 u - h(|\nabla f|)(u - \nabla f) \quad \text{– (7a)}$$

$$u(x,0) = \nabla f(x) \quad \text{– (7b)}$$

where, u_t denotes the partial derivative of u(x,t) with respect to t, ∇^2 is the Laplacian operator (applied to each spatial component of u separately), and f is an edge map that has a higher value at the desired object boundary. The functions in "g" and "h" control the amount of diffusion in GVF. In Eq.(7), $g(|\nabla f|)\nabla^2 u$ produces a smoothly varying vector field, and hence called as the "smoothing term", while $h(|\nabla f|)(u - \nabla f)$ encourages the vector field u to be close to ∇f computed from the image data and hence called as the data term. The weighting functions $g(\cdot)$ and $h(\cdot)$ apply to the smoothing and data terms respectively and they are chosen as $g(|\nabla f|) = m$ and $h(|\nabla f|) = |\nabla f|^2$ [7]. $g(\cdot)$ is constant here, and smoothing occurs everywhere, while $h(\cdot)$ grows larger near strong edges and dominates at boundaries. Hence, the Gradient Vector Flow field is defined as the vector field v(x,y)=[*u*(x,y),*v*(x,y)] that minimizes the energy functional

$$e = \int\int m(u_x^2 + u_y^2 + v_x^2 + v_y^2) + |\nabla f|^2 |v - \nabla f|^2 \, dxdy \quad \text{-- (8)}$$

The effect of this variational formulation is that the result is made smooth when there is no data.

When the gradient of the edge map is large, it keeps the external field nearly equal to the gradient, but keeps field to be slowly varying in homogeneous regions where the gradient of the edge map is small, i.e., the gradient of an edge map ∇f has vectors point toward the edges, which are normal to the edges at the edges, and have magnitudes only in the

immediate vicinity of the edges, and in homogeneous regions ∇f is nearly zero. μ is a regularization parameter that governs the tradeoff between the first and the second term in the integrand in Eq.(8). The solution of Eq.(8) can be done using the Calculus of Variations and further by treating u and v as functions of time, solving them as generalized diffusion equations [7].

5. DISCRETE COSINE TRANSFORM (DCT) BASED GVF ACTIVE CONTOURS

Transform theory plays a fundamental role in image processing. The transform of an Image yields more insight into the properties of the image. The Discrete Cosine Transform has excellent energy compaction. Hence, the Discrete Cosine Transform promises better description of the image properties. The Discrete Cosine Transform is embedded into the GVF Active Contours. When the image property description is significantly low, this helps the contour model to give significantly better performance by utilizing the energy compaction property of the DCT.

The 2D DCT is defined as

$$C(u,v) = a(u)a(v)\sum_{x=0}^{N-1}\sum_{y=0}^{N-1} f(x,y)\cos\left[\frac{(2x+1)up}{2N}\right]\cos\left[\frac{(2y+1)vp}{2N}\right] \quad \text{-- (11)}$$

The local contrast of the Image at the given pixel location (k,l) is given by

$$P(k,l) = \frac{\sum_{t=1}^{2(2n+1)-1} w_t E_t}{d_{00}} \quad \text{-- (12) where,} \quad E_t = \frac{\sum |d_{u,v}|}{N} \quad \text{-- (13) and} \quad N = \begin{cases} t+1 & t<2n+1 \\ 2(2n+1)-t & t\geq 2n+1 \end{cases} \quad \text{-- (14)}$$

Here, w_t denotes the weights used to select the DCT coefficients. The local contrast P(k,l) is then used to generate a DCT contrast enhanced Image[9], which is then subject to selective segmentation by the energy compact gradient vector flow active contour model using Eq.(8).

6. CHARACTERIZATION AND DISCUSSION

The chromosome metaphase image (size 480 x 512 pixels at 72 pixels per inch resolution) provided by Prof.Ken Castleman and Prof.Qiang Wu (Advanced Digital Imaging Research, Texas) was taken and preprocessed. Insignificant and unnecessary regions in the image were removed interactively. Interactive selection of the chromosome of interest was done by selecting a few points around the chromosome that formed the vertices of a polygon. On constructing the perimeter of the polygon, seed points for the initial contour were determined automatically by periodically selecting every third pixel along the perimeter of the polygon.

Fig. 1 Original Chromosome Image (Courtesy: Prof. Ken Castleman and Prof. Qiang Wu, Advanced Digital Imaging Research, Texas)

The GVF deformable curve was then allowed to deform until it converged to the chromosome boundary. The optimum parameters for the deformable curve with respect to the Chromosome images were determined by tabulated studies. The image was made to undergo minimal preprocessing so as to achieve the goal of boundary mapping in chromosome images with very weak edges. The DCT based GVF Active contour is govemed by the following parameters, namely, s, µ, a, ß and ?.

s determines the Gaussian filtering that is applied to the image to generate the external field. Larger value of s will cause the boundaries to become blurry and distorted, and can also cause a shift in the boundary location. However, large values of s are necessary to increase the capture range of the active contour. µ is a regularization parameter in Eq.(8), and requires a higher value in the presence of noise in the image. a determines the tension of the active contour and ß determines the rigidity of the contour. The tension keeps the active contour contracted and the rigidity keeps it smooth. a and ß may also take on value zero implying that the influence of the respective tension and rigidity terms in the diffusion equation is low. ? is the external force weight that determines the strength of the external field that is applied. The iterations were set suitably.

6.1 GRAPHICAL CHARACTERIZATION RESULTS

DCT based GVF Active Contours were used to boundary chromosome images from chromosome spread images. A few samples are presented here.

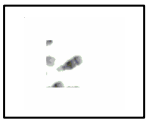
Fig.2a Sample 1


Fig.3a Sample 2


Fig.4a Sample 3


Fig. 5a Sample 4


Fig. 6a Sample 5


Fig. 7a Sample6

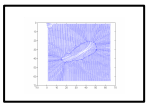
Fig.2b Vector Field

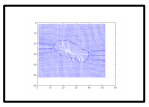
Fig.3b Vector Field

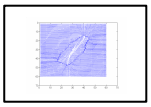
Fig.4b Vector Field

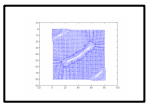
Fig.5b Vector Field

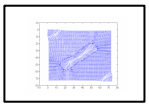
Fig.6b Vector Field

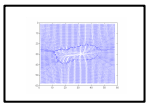
Fig.7b Vector Field


Fig.2c Output

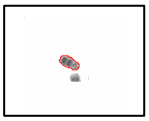
Fig.3c Output

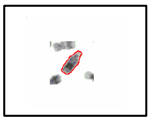
Fig.4c Output


Fig.5c Output


Fig.6c Output Image


Fig.7c Output Image

The figures show original chromosome image samples, their corresponding DCT based GVF fields and boundary mapped chromosome images as output images. For example, Fig.2a shows an original chromosome image sample, Fig.2b shows its corresponding Vector Field and Fig.2c shows its boundary mapped output image, and henceforth.

The graphical outputs show successful boundary mapping of chromosome images using DCT based GVF Active Contours.

6.2 VALIDATION OF CHARACTERIZATION EXPERIMENTS

In order to quantify the performance of a segmentation method, validation experiments are necessary. Validation is typically performed using one or two different types of truth models. In this work, ground truth model is not available and hence validation is performed on ordinal or ranking scale and then quantified. A set of 10 random samples is taken and characterization of each parameter is done. The outputs were tabulated in ranking order with "1" describing the best quality output and as the quality decreases the rank increases up to rank "97". Rank "98" is a special case, where the output image is rejected based on quality or the output image is not available due to numerical instability possibly caused due to the greater number of contour points[8]. The tables represent characterization studies for each parameter.

Each table denotes variation for only one parameter either between the lower and upper limits of the parameter or between the lower and upper limits giving significantly different output, with the other parameters taking a constant value. Hence, the best parameter value of that table is the one that gives maximum good quality outputs for all samples or a majority of samples, and exhaustive study on every parameter is done by treating the other parameters as constants.

The statistical median is used to judge the distribution of values for each parameter value for all samples. When the median leans towards the lower values, i.e., towards "1", it indicates that almost 50% of the outputs lean towards "1", making that particular parameter value an optimal one and that optimal value is chosen. The characterization studies reveal that each parameter sometimes has an optimal range within which it can assume any value thereby giving majority good outputs for all samples. But for the sake of experimental purposes, only the investigated discrete value of each parameter that gave best output was chosen. An important point to be noted is that characterization studies have been performed for those parameter values which give either significant output or significant difference in performance between adjacent parameter values. Those parameter values where there is no significant difference between adjacent parameter values have not been tabulated. Also, those parameter values outside the tabulated range which gave no proper results have not been tabulated.

Table.1 Characterization of Sigma

Sample No.	GVF (DCT) s									
	0.05	0.1	0.15	0.2	**0.25**	0.5	0.6	0.8	1	1.2
1	77	77	77	77	**77**	29	77	29	13	77
2	77	77	77	29	**13**	13	13	13	29	77
3	97	77	34	29	**77**	29	78	81	75	78
4	77	77	29	29	**31**	70	79	79	79	78
5	97	97	97	97	**98**	98	98	98	98	98
6	86	86	46	38	**38**	14	38	38	46	78
7	97	97	97	97	**98**	98	98	98	98	98
8	86	86	86	54	**98**	98	98	98	98	98
9	77	77	77	77	**38**	46	15	77	13	79
10	86	77	13	77	**46**	65	78	13	78	77
Median	86	77	77	**66**	**62**	**55**	78	78	77	78

In Table 1, the median indicates that the acceptable optimal range of s is 0.2 to 0.5. The best value compared qualitatively amongst those tested is 0.25 and hence it is chosen for performing further characterization.

Table 2. Characterization of Mu

Sample No.	GVF (DCT) μ					
	0.05	**0.075**	0.09375	0.1125	0.15	0.3
1	23	**21**	21	23	23	97
2	21	**5**	23	23	23	97
3	30	**29**	29	46	50	97
4	23	**23**	23	40	23	97
5	98	**98**	98	97	97	97
6	48	**40**	48	48	46	97
7	98	**98**	50	50	34	97
8	98	**89**	62	97	97	97
9	71	**86**	30	71	71	97
10	23	**21**	29	71	23	97
Median	**39**	**35**	**29**	49	40	97

In Table 2, the median indicates that the acceptable optimal range of μ is 0.05 to 0.09375. The best value compared qualitatively amongst those tested is 0.075 and hence it is chosen for performing further characterization.

Table 3. Characterization of Alpha

Sample No.	GVF (DCT) a				
	0	0.125	0.25	0.5	1
1	**7**	23	77	71	77
2	**7**	30	29	77	30
3	**5**	67	78	78	67
4	**23**	23	79	80	80
5	**98**	98	98	98	97
6	**98**	48	40	46	87
7	**98**	98	98	97	97
8	**90**	86	62	97	94
9	**21**	23	23	71	27
10	**5**	7	23	21	71
Median	**22**	**39**	70	78	79

In Table 3, the median indicates that the acceptable optimal range of a extends from 0 to 0.125. The best value compared qualitatively amongst those tested is 0 and hence it is chosen for performing further characterization.

Table 4. Characterization of Beta

Sample No.	GVF (DCT) ß		
	0	0.5	1
1	**23**	30	71
2	**5**	21	21
3	**5**	21	31
4	**21**	23	71
5	**98**	98	98
6	**98**	46	70
7	**98**	98	98
8	**38**	94	13
9	**23**	71	71
10	**3**	21	30
Median	**23**	**38**	71

In Table 4, the median indicates that the acceptable optimal range of ß extends from 0 to 0.5. The best value compared qualitatively amongst those tested is 0 and hence it is chosen for performing further characterization.

Table 5. Characterization of Kappa

Sample No.	GVF (DCT) ?					
	0	0.5	**0.625**	0.75	0.875	1
1	97	7	**5**	5	5	5
2	97	3	**3**	3	1	1
3	97	21	**19**	21	30	67
4	97	7	**7**	7	23	71
5	97	98	**98**	98	98	98
6	97	98	**98**	98	86	98
7	97	98	**98**	98	98	98
8	97	86	**98**	97	98	82
9	97	7	**7**	23	23	21
10	97	21	**5**	19	19	21
Median	97	**21**	**13**	**22**	**26**	69

In Table 5, the median indicates that the acceptable optimal range of ? extends from 0.5 to 0.875. The best value compared qualitatively amongst those tested is 0.625.

Hence the optimal set of parameter values that give good boundary mapping for the given class of chromosome images is s = 0.25, µ = 0.075, a = 0, ß = 0, and ? = 0.625. A safe limit of 5% tolerance can be introduced to the optimal range of parameter values to make them suitable for use in similar classes of chromosome spread images (indicated in Table 6).

Table 6. Optimal range of DCT based GVF Active Contour parameter values for tested chromosome spread images

Parameter	**Parameter Value used for tested spread image**	**Acceptable Range of Parameter values**	**Acceptable Range of Values at 5% tolerance**
GVF (DCT) s	0.25	[0.2 , 0.5]	[0.1900 , 0.5250]
GVF (DCT) µ	0.075	[0.05 , 0.09375]	[0.0475 , 0.0984]
GVF (DCT) a	0	[0 , 0.125]	[0.0000 , 0.1313]
GVF (DCT) ß	0	[0 , 0.5]	[0.0000 , 0.5250]
GVF (DCT) ?	0.625	[0.5 , 0.875]	[0.4750 , 0.9187]

6.3 STATISTICAL VALIDATION OF CHARACTERIZATION EXPERIMENTS

The parameters act independently on the boundary mapping scheme. In each characterization, the effect of other parameters will also be felt as they assume a definite constant value. In the course of the characterization study from Table 1 to Table 5, optimum values for the respective parameters are chosen and applied as constant in the characterization study of the next parameter in the successive table. In the last characterization study shown in Table 5, the values of s, µ, a and ß take on the chosen optimal values and only ? is investigated, thereby yielding a one way variation. Hence, one way analysis of variance on Table 5 is sufficient to test the significance of the entire boundary mapping process. A significant outcome from Table 5 will justify that the experimental results of Table 5 are valid, implying that the selected parameter values from Table 1 to Table 4 used as constants in Table 5 are also valid.

Hence, one way Anova test is performed on the last characterization (Table 5) to judge the experimental results. At the customary .05 significance level, one way Anova test yields a p value of 7.17082E-08 on Table 5, which rejects the null hypothesis. The very small p-value of 7.17082E-08 indicates that differences between the column means are highly significant. The probability of this outcome under the null hypothesis is less than 8 in 100,000,000. The test therefore strongly supports the alternate hypothesis that one or more of the samples are drawn from populations with different means. This implies that the results in Table 5 do not arise out of mere fluctuations and the results are actually significant. Therefore the experimental results are valid. This justifies that a suitable value of parameter ? can be chosen from Table 5, and that the constant values of parameters s, µ, a, and ß used in Table 5 are also valid as these values also have significant influence on the results tabulated in Table 5. Therefore, the experimental results and the inferences are also significant.

7. STANDARDIZATION

Characterization studies have yielded an acceptable optimal range of values for the parameters s,µ,a,ß and ?. To establish that the parameter values are standardized with reference to similar classes of chromosome spread images, standardization experiments are carried out in a similar class of chromosome spread images from a different dataset, made available by the kind courtesy of Dr.Michael Difilippantonio, Staff Scientist at the Section of Cancer Genomics, Genetics Branch / CCR / NCI / NIH, Bethesda MD.

The same characterized parameter values of s = 0.25, µ = 0.075, a = 0, ß = 0, and ? = 0.625 have been used. Good boundary mapping results have been obtained and the results are shown in the following pages. Each sample is unique as the chromosomes are imaged in a fluid medium, and random bending effects are manifested. Hence it is shown that the DCT based GVF Active Contour, governed by the characterized values of the parameters of s = 0.25, µ = 0.075, a = 0, ß = 0, and ? = 0.625 are able to overcome the variations in the shape of the chromosomes and give good boundary mapping in each of the samples.

A few samples are illustrated in the following pages. The chromosome image is seen in gray scale, while the DCT based GVF Active Contour mapped boundary is shown in red.

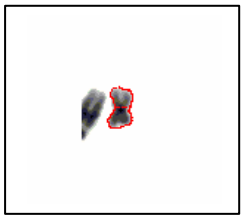

Fig.8 Sample1

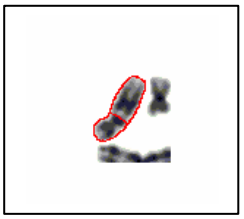

Fig.9 Sample2

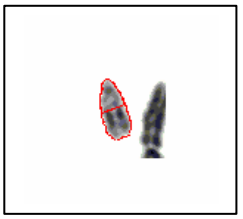

Fig.10 Sample3

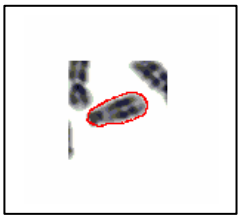

Fig.11 Sample4

Fig.12 Sample5

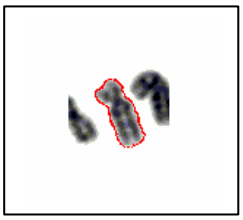

Fig.13 Sample6

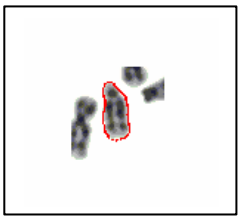

Fig.14 Sample7

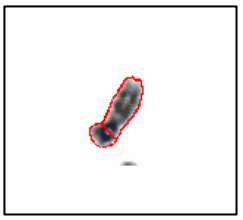

Fig.15 Sample8

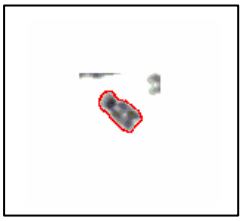

Fig.16 Sample9

Fig.17 Sample10

Fig.18 Sample11

Fig.19 Sample12

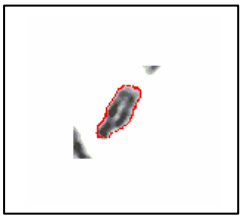

Fig.20 Sample13

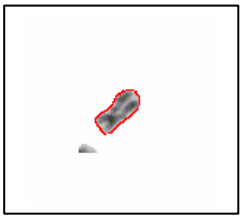

Fig.21 Sample14

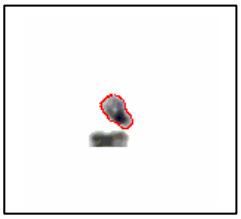

Fig.22 Sample15

Fig.23 Sample16

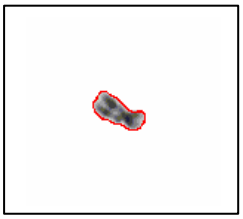

Fig.24 Sample17

Fig.25 Sample18

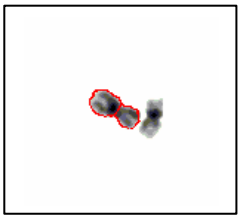

Fig.26 Sample19

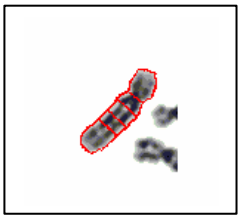

Fig.27 Sample20

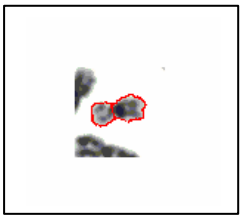

Fig.28 Sample21

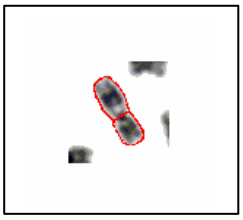

Fig.29 Sample22

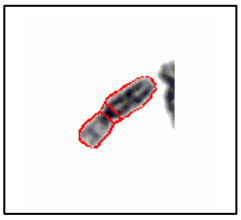

Fig.30 Sample23

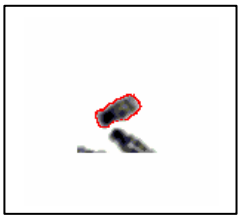

Fig.31 Sample24

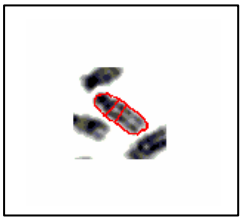

Fig.32 Sample25

Fig.33 Sample26

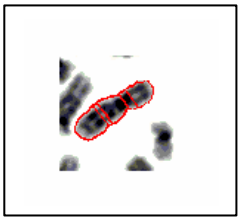

Fig.34 Sample27

Fig.35 Sample28

Fig.36 Sample29

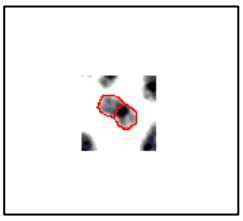

Fig.37 Sample30

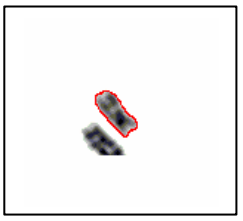

Fig.38 Sample31

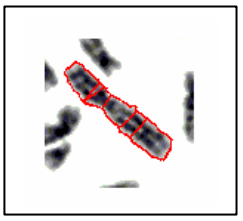

Fig.39 Sample32

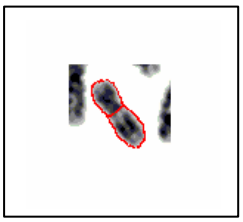

Fig.40 Sample33

Fig.41 Sample34

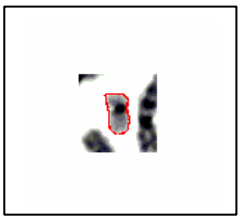

Fig.42 Sample35

Fig.43 Sample36

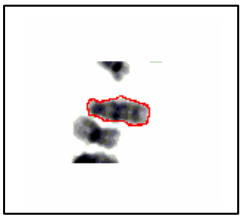

Fig.44 Sample37

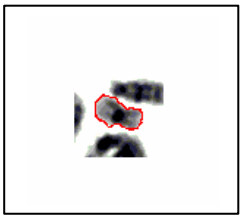

Fig.45 Sample38

Fig.46 Sample39

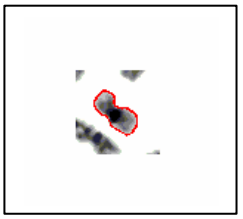

Fig.47 Sample40

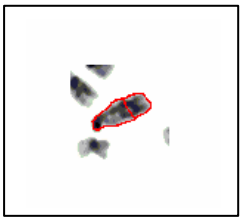

Fig.48 Sample41

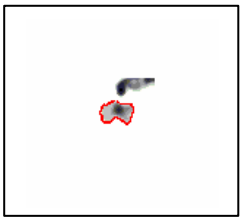

Fig.49 Sample42

Fig. 50 Sample43

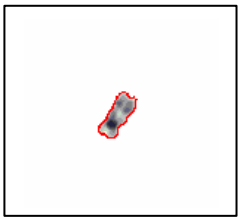

Fig.51 Sample44

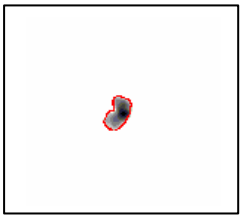

Fig.52 Sample45

Fig.53 Sample46

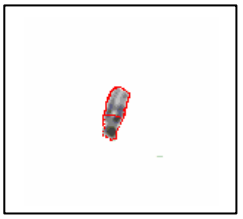

Fig.54 Sample47

Fig.55 Sample48

Fig.56 Sample49

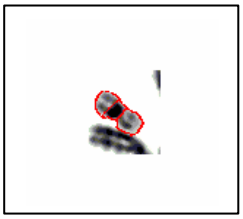

Fig.57 Sample50

Fig.58 Sample51

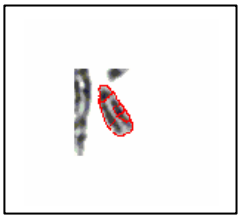

Fig.59 Sample52

Fig.60 Sample53

Fig.61 Sample54

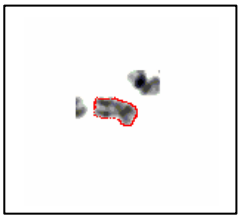

Fig.62 Sample55

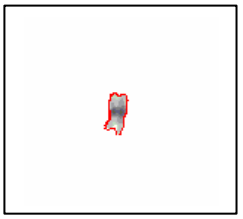

Fig.63 Sample56

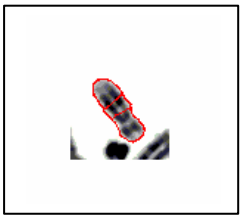

Fig.64 Sample57

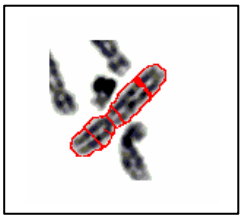

Fig.65 Sample58

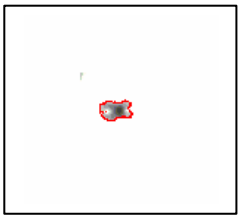

Fig.66 Sample59

Fig.67 Sample60

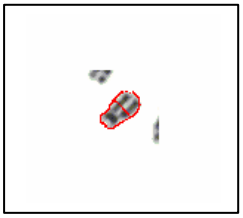

Fig.68 Sample61

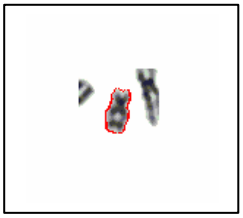

Fig.69 Sample62

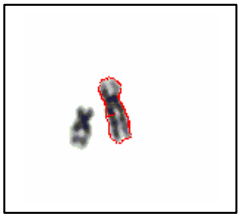

Fig.70 Sample63

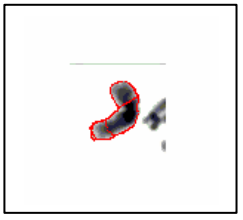

Fig.71 Sample64

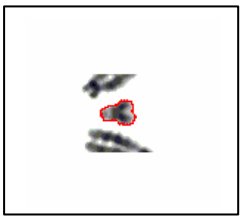

Fig.72 Sample65

Fig.73 Sample66

Fig.74 Sample67

Fig.75 Sample68

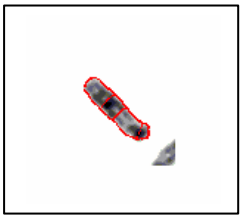

Fig.76 Sample69

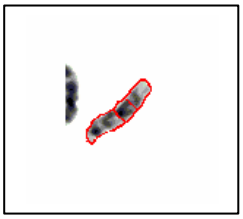

Fig.77 Sample70

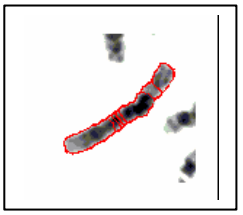

Fig.78 Sample71

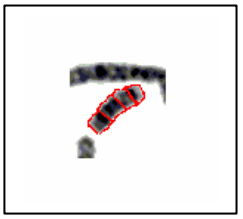

Fig.79 Sample72

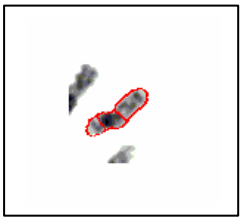

Fig.80 Sample73

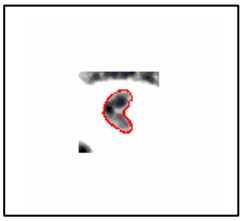

Fig.81 Sample74

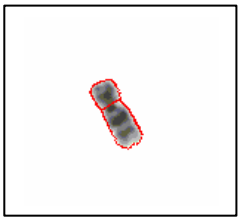

Fig.82 Sample75

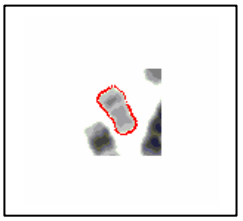

Fig.83 Sample76

Fig.84 Sample77

Fig.85 Sample78

Fig.86 Sample79

Fig.87 Sample80

Fig.88 Sample81

Fig.89 Sample82

Fig.90 Sample83

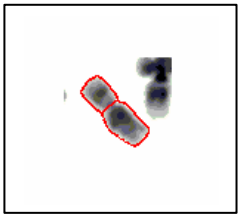

Fig.91 Sample84

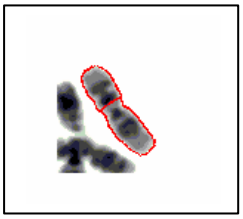

Fig.92 Sample85

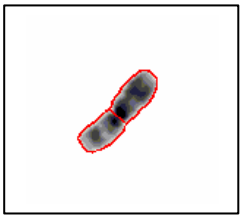

Fig.93 Sample86

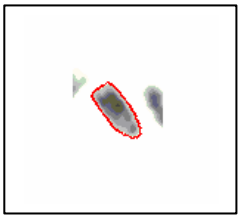

Fig.94 Sample87

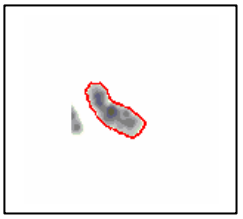

Fig.95 Sample88

Fig.96 Sample89

Fig.97 Sample90

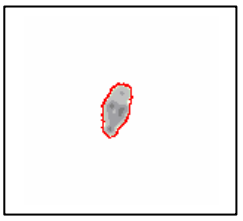

Fig.98 Sample91

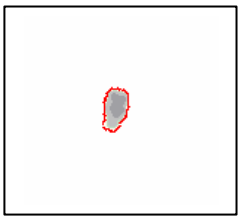

Fig.99 Sample92

Fig.100 Sample93

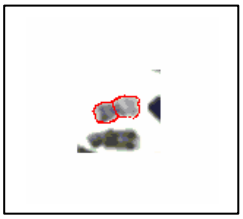

Fig.101 Sample94

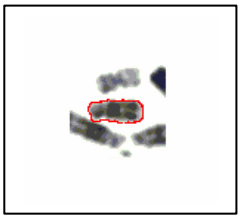

Fig.102 Sample95

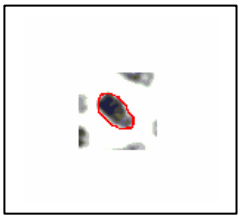

Fig.103 Sample96

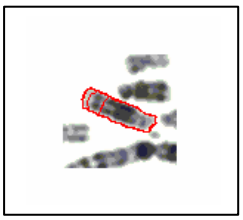

Fig.104 Sample97

Fig.105 Sample98

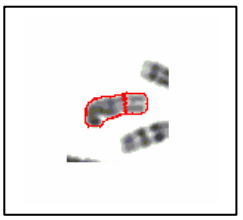

Fig.106 Sample99

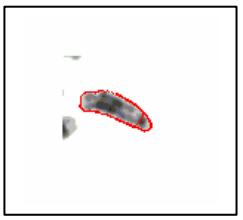

Fig.107 Sample100

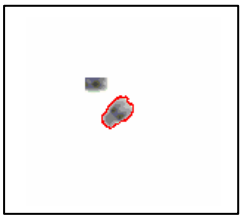

Fig.108 Sample101

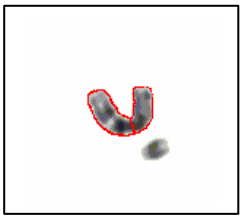

Fig.109 Sample102

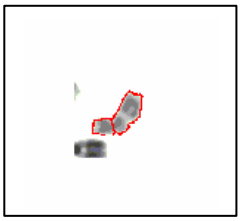

Fig.110 Sample103

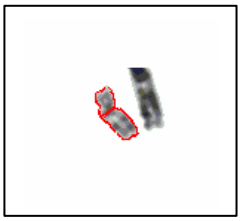

Fig.111 Sample104

Fig.112 Sample105

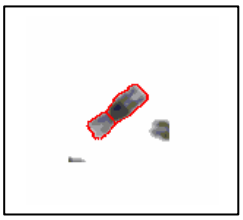

Fig.113 Sample106

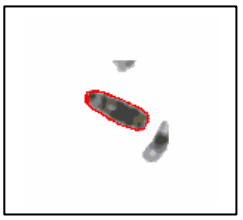

Fig.114 Sample107

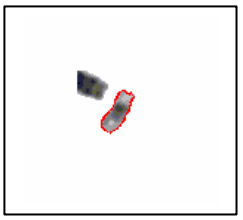

Fig.115 Sample108

Fig.116 Sample109

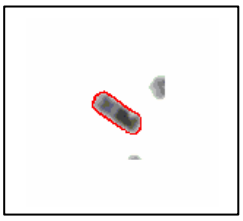

Fig.117 Sample110

Fig.118 Sample111

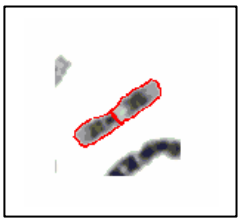

Fig.119 Sample112

Fig.120 Sample113

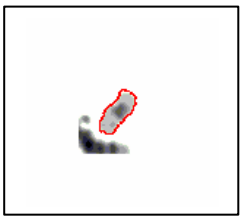

Fig.121 Sample114

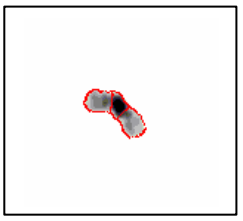

Fig.122 Sample115

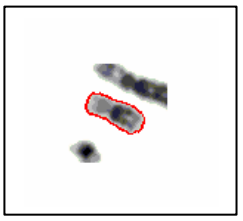

Fig.123 Sample116

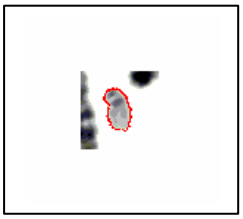

Fig.124 Sample117

Fig.125 Sample118

Fig.126 Sample119

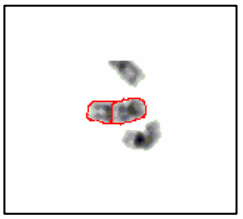

Fig.127 Sample120

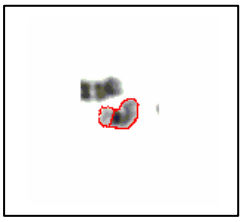

Fig.128 Sample121

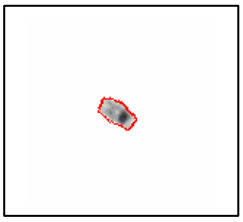

Fig.129 Sample122

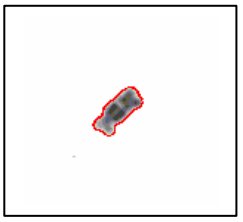

Fig.130 Sample123

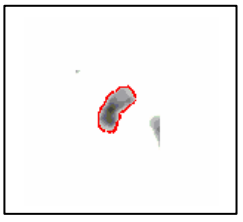

Fig.131 Sample124

Fig.132 Sample125

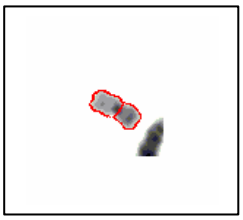

Fig.133 Sample126

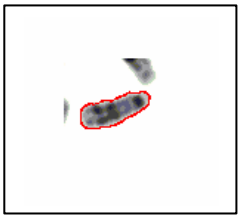

Fig.134 Sample127

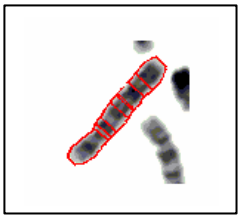

Fig.135 Sample128

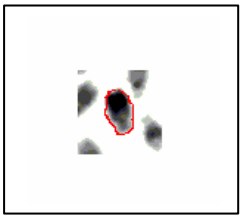

Fig.136 Sample129

Fig.137 Sample130

Fig.138 Sample131

Fig.139 Sample132

Fig.140 Sample133

Fig.141 Sample134

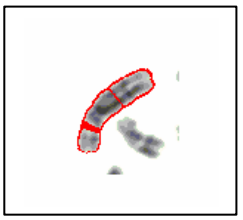

Fig.142 Sample135

Fig.143 Sample136

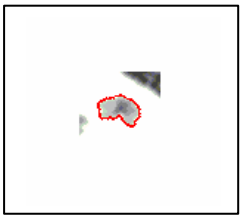

Fig.144 Sample137

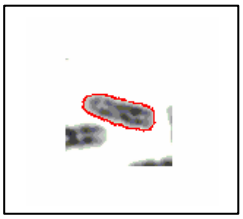

Fig.145 Sample138

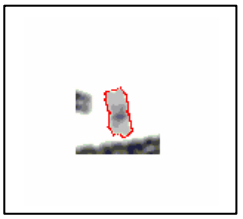

Fig.146 Sample139

Fig.147 Sample140

Fig.148 Sample141

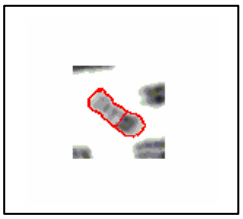

Fig.149 Sample142

Fig.150 Sample143

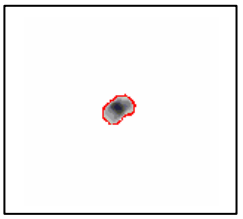

Fig.151 Sample144

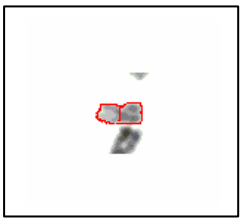

Fig.152 Sample145

Fig.153 Sample146

Fig.154 Sample147

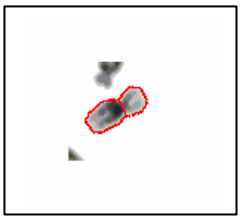

Fig.155 Sample148

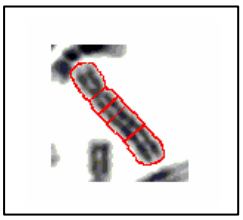

Fig.156 Sample149

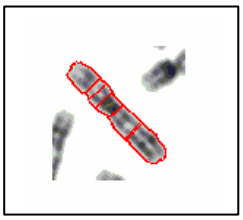

Fig.157 Sample150

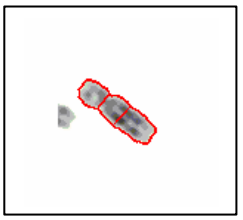

Fig.158 Sample151

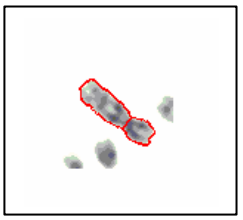

Fig.159 Sample152

From the above graphical illustrations of boundary mapped chromosomes, it is inferred that the set of parameter values s = 0.25, μ = 0.075, a = 0, ß = 0, and ? = 0.625 governing the formu lation of the DCT based GVF Active Contours are hence standardized, and can be applied to obtain successful boundary mapping in similar classes of chromosome spread images.

8. EVALUATION OF STANDARDIZATION

To assess the success of the standardization, the DCT based GVF Active Contours with the same characterized values of the parameters were applied to boundary map chromosome spread images from a different dataset, which was made available by the kind courtesy of Prof.Ekaterina Detcheva, at the Artificial Intelligence Department, Institute of Mathematics and Informatics, Sofia, Bulgaria.

A few graphical results are presented subsequently, which indicate that the standardization has been successful. The chromosome is shown in gray scale and the mapped boundary is indicated in red color.

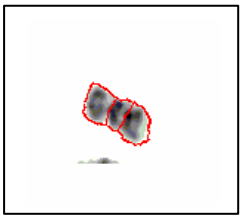

Fig.160 Sample 1

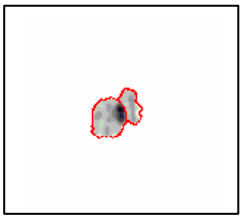

Fig.161 Sample 2

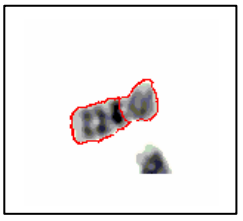

Fig.162 Sample 3

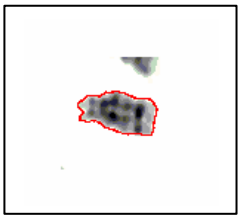

Fig.163 Sample 4

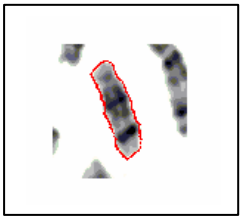

Fig.164 Sample 5

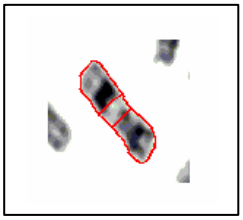

Fig.165 Sample 6

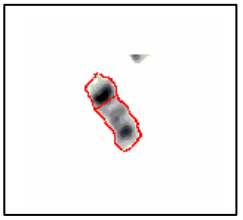

Fig.166 Sample 7

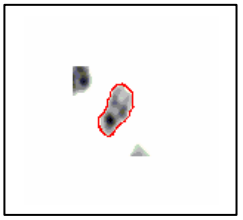

Fig.167 Sample 8

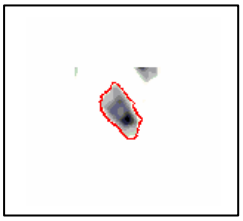

Fig.168 Sample 9

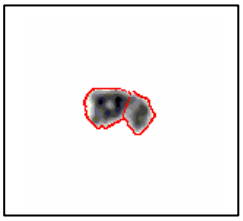

Fig.169 Sample 10

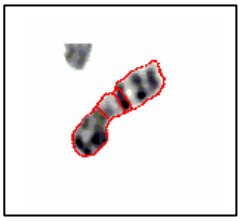

Fig.170 Sample 11

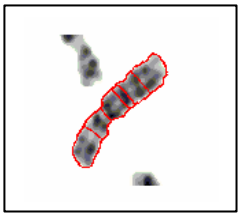

Fig.171 Sample 12

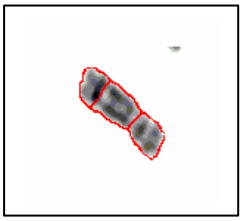

Fig.172 Sample 13

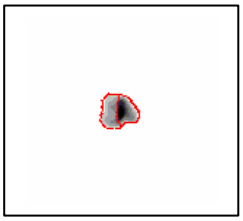

Fig.173 Sample 14

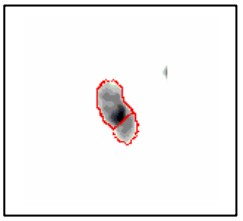

Fig.174 Sample 15

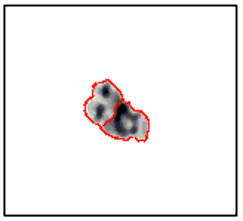

Fig.175 Sample 16

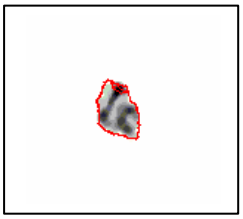

Fig.176 Sample 17

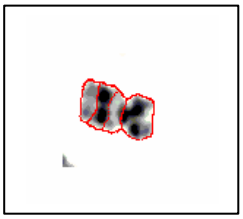

Fig.177 Sample 18

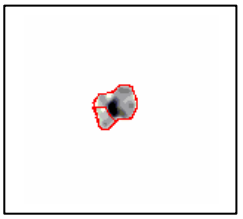

Fig.178 Sample 19

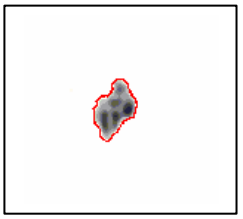

Fig.179 Sample 20

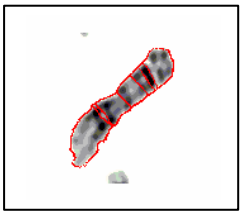

Fig.180 Sample 21

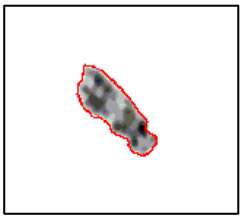

Fig.181 Sample 22

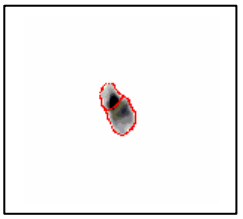

Fig.182 Sample 23

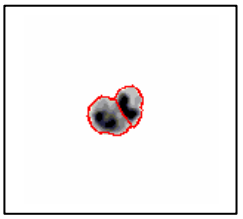

Fig.183 Sample 24

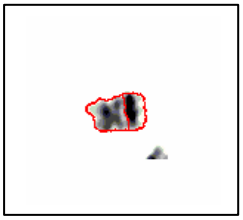

Fig.184 Sample 25

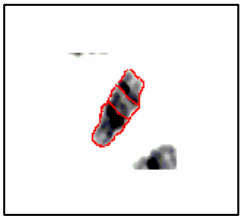

Fig.185 Sample 26

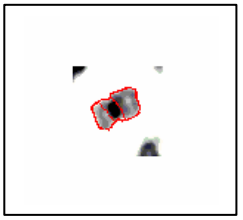

Fig.186 Sample 27

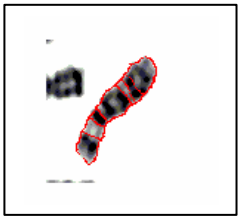

Fig.187 Sample 28

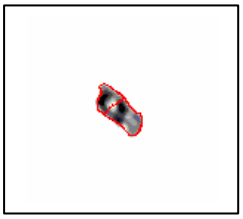

Fig.188 Sample 29

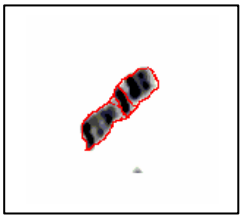

Fig.189 Sample 30

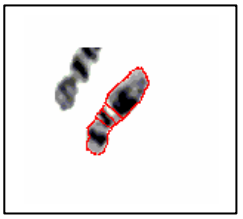

Fig.190 Sample 31

Fig.191 Sample 32

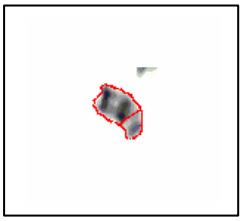

Fig.192 Sample 33

Fig.193 Sample 34

Fig.194 Sample 35

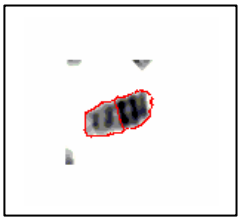

Fig.195 Sample 36

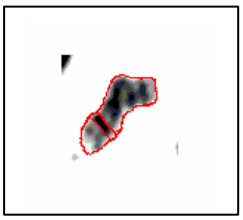

Fig.196 Sample 37

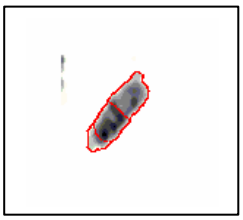

Fig.197 Sample 38

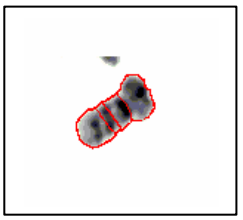

Fig.198 Sample 39

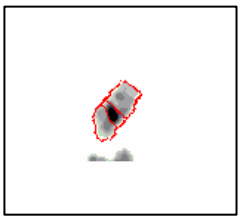

Fig.199 Sample 40

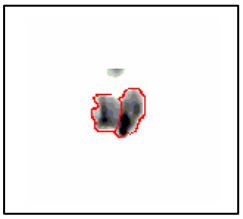

Fig.200 Sample 41

Fig.201 Sample 42

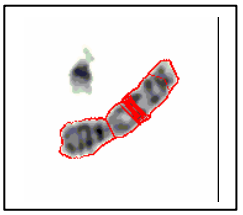

Fig.202 Sample 43

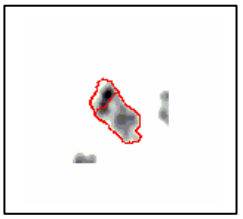

Fig.203 Sample 44

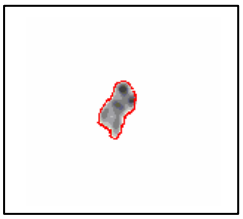

Fig.204 Sample 45

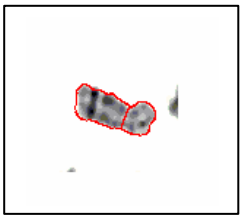

Fig.205 Sample 46

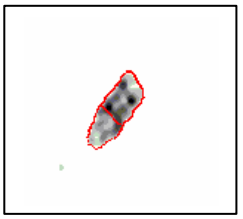

Fig.206 Sample 47

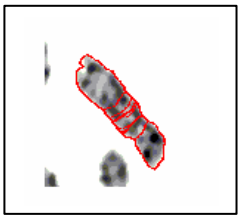

Fig.207 Sample 48

Hence, it is established that the characterized parameter values, when applied to govern the DCT based GVF Active Contours on independent datasets of chromosome spread images are able to successfully boundary map chromosome

spread images. They have successfully passed the test of standardization and also the test of evaluation of standardization.

The boundary mapping scheme is subjected to intense testing using another dataset, available at http://worms.zoology.wisc.edu/zooweb/Phelps/karyotype.html by the kind courtesy of Wisconsin State Laboratory of Hygiene. The same characterized parameter values are used here in DCT based GVF Active Contours. A few boundary mapped results from the Wisconsin State Laboratory of Hygiene dataset is shown below.

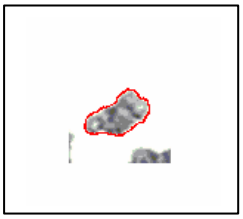

Fig. 208 Sample 1

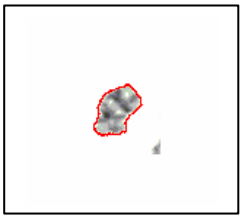

Fig. 209 Sample 2

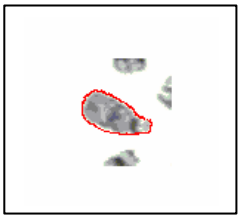

Fig. 210 Sample 3

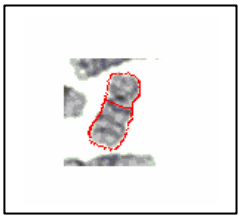

Fig. 211 Sample 4

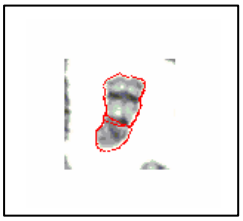

Fig. 212 Sample 5

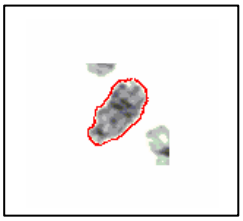

Fig. 213 Sample 6

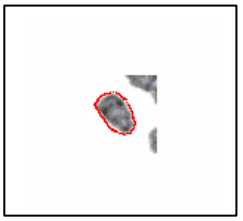

Fig. 214 Sample 7

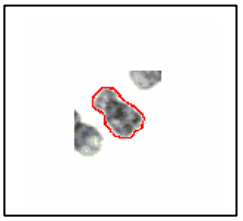

Fig. 215 Sample 8

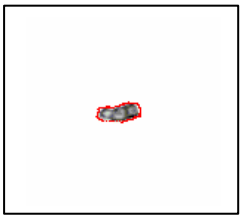

Fig. 216 Sample 9

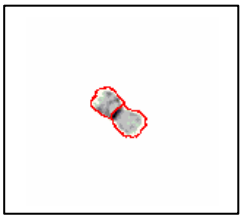

Fig. 217 Sample 10

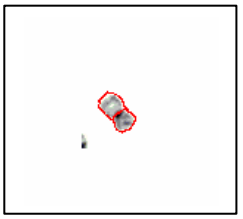

Fig. 218 Sample 11

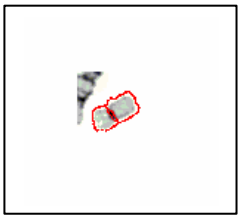

Fig. 219 Sample 12

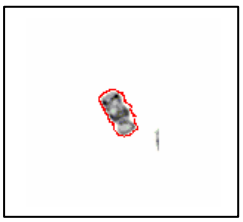

Fig. 220 Sample 13

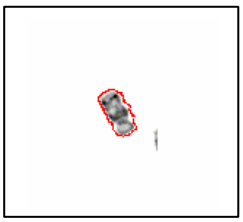

Fig. 221 Sample 14

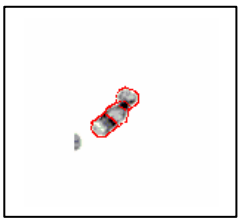

Fig. 222 Sample 15

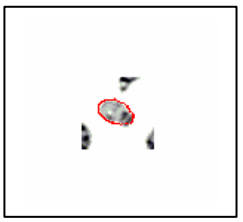

Fig. 223 Sample 16

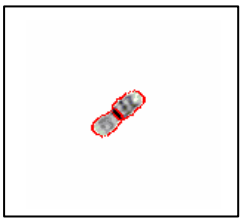

Fig. 224 Sample 17

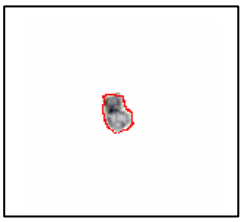

Fig. 225 Sample 18

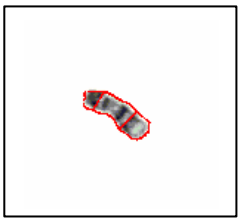

Fig. 226 Sample 19

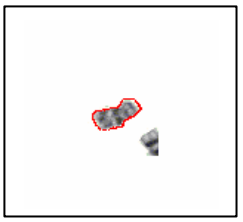

Fig. 227 Sample 20

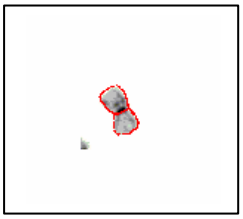

Fig. 228 Sample 21

Fig. 229 Sample 22

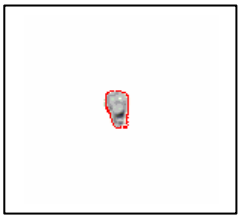

Fig. 230 Sample 23

Fig. 231 Sample 24

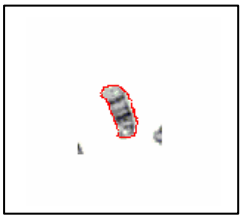

Fig. 232 Sample 25

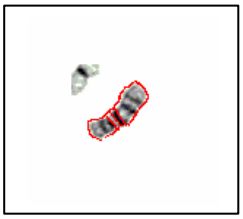

Fig. 233 Sample 26

Fig. 234 Sample 27

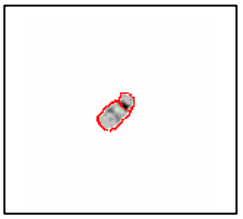

Fig. 235 Sample 28

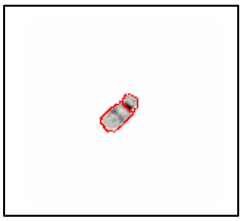

Fig. 236 Sample 29

Fig. 237 Sample 30

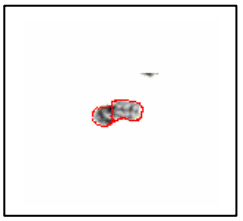

Fig. 238 Sample 31

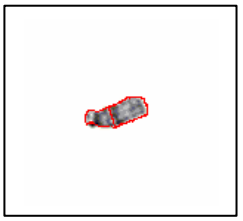

Fig. 239 Sample 32

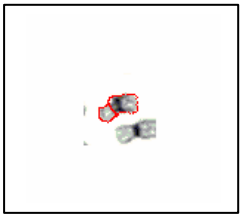

Fig. 240 Sample 33

Fig. 241 Sample 34

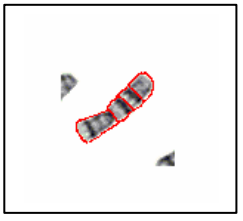

Fig. 242 Sample 35

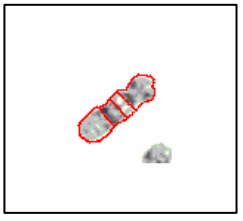

Fig. 243 Sample 36

Fig. 244 Sample 37

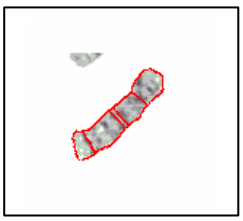

Fig. 245 Sample 38

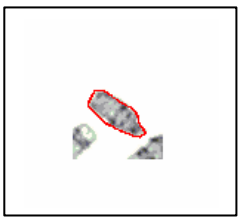

Fig. 246 Sample 39

Fig. 247 Sample 40

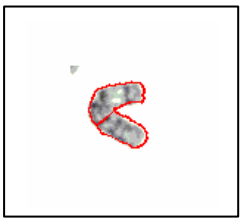

Fig. 248 Sample 41

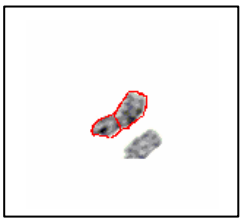

Fig. 249 Sample 42

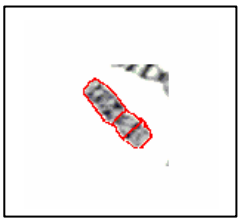

Fig. 250 Sample 43

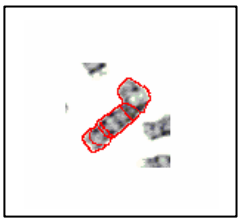

Fig. 251 Sample 44

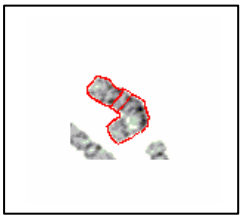

Fig. 252 Sample 45

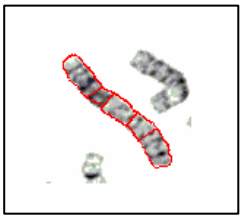

Fig. 253 Sample 46

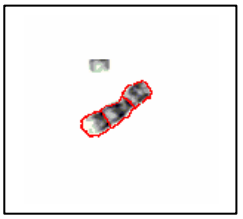

Fig. 254 Sample 47

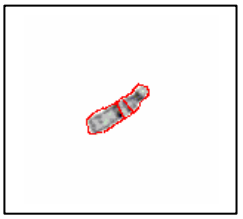

Fig. 255 Sample 48

The graphical results that the characterized parameters in DCT based GVF Active Contours are able to successfully and accurately boundary map chromosome spread images in this dataset also. Hence, it is established that the characterized parameters are truly standardized, i.e., they perform boundary mapping efficiently independent of the dataset from which the chromosome spread images are obtained. It is therefore inferred that the parameters are able to overcome the variability in shape, features, image properties and imaging conditions.

Therefore, the DCT based GVF Active Contours are established as an efficient tool for boundary mapping in chromosome spread images.

9. CONCLUSION

The Discrete Cosine Transform based Gradient Vector Flow Active Contour is an efficient tool for boundary mapping chromosome spread images and can be used for successful boundary mapping of chromosome spread images from any dataset.

The values s = 0.25, μ = 0.075, a = 0, ß = 0, and ? = 0.625 have hence been standardized and evaluated. They are independent of the dataset from which the chromosome spread images are derived, thus making them independent of shape variations, image property variations, and imaging condition variations. Therefore, the standardized parameters

can be used in DCT based GVF Active Contours for successful and efficient boundary mapping of chromosome spread images.

10. ACKNOWLEDGMENT

The authors express their thanks to **Dr.Michael Difilippantonio**, *Staff Scientist at the Section of Cancer Genomics, Genetics Branch/ CCR / NCI / NIH, Bethesda MD*; **Prof.Ekaterina Detcheva** at the *Artificial Intelligence Department, Institute of Mathematics and Informatics, Sofia, Bulgaria*; **Prof.Ken Castleman** and **Prof.Qiang Wu**, from *Advanced Digital Imaging Research, Texas* for their help in providing chromosome spread images.

The authors thank **Wisconsin State Laboratory of Hygiene** for the chromosome spread images available at *http://worms.zoology.wisc.edu/zooweb/Phelps/karyotype.html*.

11. REFERENCES

[1] A.J.Abrantes and J.S.Marques, "A class of constrained clustering algorithms for object boundary extraction", IEEE Trans. on Image Processing, 5(11):1507-1521, November 1996.

[2] B.Leroy, I.Herlin and L.D.Cohen, "Multi-resolution algorithms for active contour models", In 12th Intl. Conf. on Analysis and Optimization of Systems: 58-65, 1996.

[3] C.Davatzikos and J.L.Prince, "An active contour model for mapping the cortex", IEEE Trans. on Medical Imaging, 14(1):65-80, March 1995.

[4] C.Davatzikos and J.L.Prince, "Convexity analysis of active contour models", In Proc. Conf. on Info. Sci. and Sys.:581-587, 1994.

[5] C. Xu and J.L. Prince, "Gradient Vector Flow: A New External Force for Snakes", IEEE Proc. Conf. on Comp. Vis. Patt. Recog. (CVPR'97) 66-71

[6] C. Xu and J.L.Prince, "Gradient Vector Flow Deformable Models", In Handbook of Medical Imaging, Academic Press, Sept. 2000

[7] C.Xu and J.L. Prince, "Snakes, shapes and gradient vector flow", IEEE Trans. on Image Processing, 7(3):359-369, March 1998.

[8] D. Rueckert, "Segmentation and tracking in cardiovascular MR images using geometrically deformable models and templates", PhD thesis, Imperial College of Science, Technology and Medicine, London, 1997.

[9] Jinshan Tang, S.T. Acton, "A DCT based gradient vector flow snake for object boundary detection", Image Analysis and Interpretation, 2004. 6th IEEE Southwest Symposium on: 157 – 161, 28-30 March 2004.

[10] J.L. Prince and C.Xu, "A new external force model for snakes", In 1996 Image and Multidimensional Signal Processing Workshop:30-31, 1996.

[11] L.D.Cohen, "On active contours and balloons", CVGIP: Image Understanding, 53(2):211-218, March 1991.

[12] L.D.Cohen and I.Cohen, "Finite-element methods for active contour models and balloons for 2-D and 3-D images", IEEE Trans. On Pattern Anal. Machine Intell., 15(11):1131-1147, November 1993.

[13] M. Kass, A. Witkin, D. Terzopoulos, "Snakes: active contour models", Int. J. Comp. Vision 1: 321–331, 1987.

[14] T. McInerney and D. Terzopoulos, "Deformable models in medical image analysis", IEEE Proceedings of the Workshop on Mathematical Methods in Biomedical Image Analysis: 171-180, 1996.